Nuclear Inst. and Methods in Physics Research, A 889 (2018) 39–46

Contents lists available at ScienceDirect

Nuclear Inst. and Methods in Physics Research, A

journal homepage: www.elsevier.com/locate/nima

A Geant4 evaluation of the Hornyak button and two candidate detectors for the TREAT hodoscope

Wenkai Fu, Priyarshini Ghosh, Mark J. Harrison, Douglas S. McGregor, Jeremy A. Roberts *

Department of Mechanical and Nuclear Engineering, Kansas State University, Manhattan, KS 66506, USA

ARTICLE INFO

Keywords:
TREAT hodoscope
Fast-neutron detection
ZnS(Ag)
Geant4
Hornyak button
Cherenkov

ABSTRACT

The performance of traditional Hornyak buttons and two proposed variants for fast-neutron hodoscope applications was evaluated using Geant4. The Hornyak button is a ZnS(Ag)-based device previously deployed at the Idaho National Laboratory's TRansient REActor Test Facility (better known as TREAT) for monitoring fast neutrons emitted during pulsing of fissile fuel samples. Past use of these devices relied on pulse-shape discrimination to reduce the significant levels of background Cherenkov radiation. Proposed are two simple designs that reduce the overall light guide mass (here, polymethyl methacrylate or PMMA), employ silicon photomultipliers (SiPMs), and can be operated using pulse-height discrimination alone to eliminate background noise to acceptable levels. Geant4 was first used to model a traditional Hornyak button, and for assumed, hodoscope-like conditions, an intrinsic efficiency of 0.35% for mono-directional fission neutrons was predicted. The predicted efficiency is in reasonably good agreement with experimental data from the literature and, hence, served to validate the physics models and approximations employed. Geant4 models were then developed to optimize the materials and geometries of two alternatives to the Hornyak button, one based on a homogeneous mixture of ZnS(Ag) and PMMA, and one based on alternating layers of ZnS(Ag) and PMMA oriented perpendicular to the incident neutron beam. For the same radiation environment, optimized, 5-cm long (along the beam path) devices of the homogeneous and layered designs were predicted to have efficiencies of approximately 1.3% and 3.3%, respectively. For longer devices, i.e., lengths larger than 25 cm, these efficiencies were shown to peak at approximately 2.2% and 5.9%, respectively. Moreover, both designs were shown to discriminate Cherenkov noise intrinsically by using an appropriate pulse-height discriminator level, i.e., pulse-shape discrimination is not needed for these devices.

1. Introduction

Interest in accident-tolerant nuclear fuels has led to the planned restart of the TRansient REActor Test Facility (TREAT) at Idaho National Laboratory (INL) [1]. The TREAT core can be pulsed to powers up to 20 GWth [2] over short periods of time, resulting in conditions similar to those expected during severe reactor accidents. The core consists of prismatic fuel elements that can be arranged with a central, voided channel that provides line-of-sight viewing through the core. In this central region, fuel samples are irradiated during large-power transients. The physical motion and deformation of the fuel sample can be monitored during such transients by detecting the fast neutrons emitted from fission within the sample. These fission neutrons pass through an inner, concrete collimator and an outer, steel collimator with over 300 milled channels at the end of which an array of fast-neutron detectors and associated electronics is situated [3]. At the detector end, the collimator channels are approximately 8 mm by 3 mm in cross-sectional area. At the other end, the channels converge to an image plane centered about the fuel sample, and thus, the signals recorded provide a "picture" of the sample evolution over time.

Hornyak buttons [4] were used as fast-neutron detectors in the original TREAT hodoscope [3]. The devices used at TREAT consist of a scintillation volume sandwiched between two polymethyl methacrylate (PMMA) light guides, as shown in Fig. 1. The scintillation volume contains a uniform mixture of ZnS(Ag) (5% by mass) and PMMA. A fast neutron entering the scintillation volume has a certain probability to interact with the hydrogen in the PMMA and to generate a recoil proton via elastic scattering. If there are ZnS(Ag) scintillator grains along the path of the recoil proton, light is emitted due to the energy deposited in the scintillator. If the light can be detected by the photomultiplier tube (PMT), a signal pulse can be generated. The polished, cylindrical light guides yield reasonably good light-collection efficiency along the

* Corresponding author.
E-mail address: jaroberts@k-state.edu (J.A. Roberts).

https://doi.org/10.1016/j.nima.2018.01.092
Received 6 July 2017; Received in revised form 26 January 2018; Accepted 28 January 2018
Available online 5 February 2018

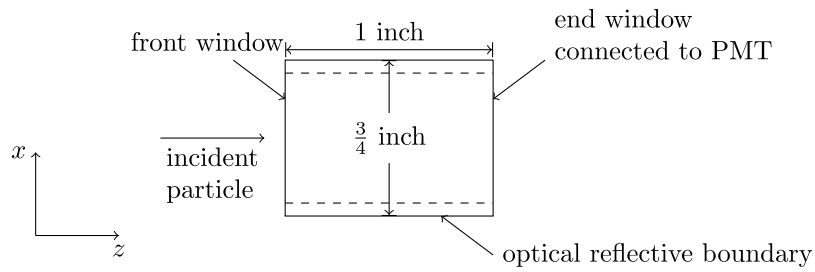

(a) Side view.

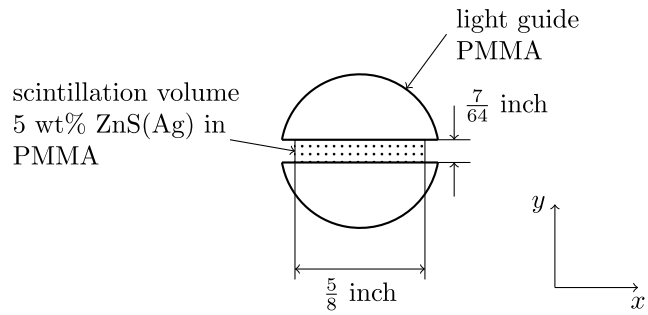

(b) Cross-section view.

Fig. 1. A geometric illustration of the Hornyak button as used at TREAT (after Ref. [3]).

1-in. length of the scintillation volume. For neutrons above 0.1 MeV, the Hornyak buttons used at TREAT were observed to have an efficiency of approximately 0.4% [3].

The radiation environment present at the detector end of the hodoscope collimator presents several challenges to measuring fast neutrons. A primary component of background radiation consists of capture gamma rays generated in the collimator steel [3]. These gamma rays may interact within the Hornyak button to generate electrons via the photoelectric effect, Compton scattering, and pair production. These electrons can subsequently lead to additional noise through electron-induced scintillation and Cherenkov radiation. Considering the relatively long range of the electrons, only a small fraction of the gamma energy is expected to be transferred to the ZnS(Ag). Therefore, the scintillation noise is relatively easy to eliminate by pulse-height discrimination. However, the Hornyak button was observed to suffer from large Cherenkov noise generated in the light guides and the photomultiplier glass envelope [3]. The overwhelming Cherenkov noise may have contributed to the nonlinearity between the detector response and the TREAT neutron monitors during large transient experiments [3]. To reject the Cherenkov noise, a pulse-shaping technique was developed based on the decay time difference between the scintillation light and the Cherenkov light [5]. Additionally, lead filters were used in front of the detectors to attenuate the gamma rays and to help eliminate the nonlinearity [3]. These techniques, though successful, complicated the detection system.

To overcome these limitations of the Hornyak button, and to develop devices with higher efficiencies, alternative technologies are under investigation at Kansas State University (KSU). Early work studied fast-sensitive, micro-structured neutron detectors (MSNDs) based on actinide reactants [6]. Reported here are two, alternative designs based on the reasonably successful Hornyak button that optimize the geometry and material arrangement of ZnS(Ag) and PMMA. The first design, like the original Hornyak button, is based on a homogeneous mixture of ZnS(Ag) in PMMA. However, rather than sandwich the scintillating volume between two PMMA light guides, silicon photomultipliers (SiPMs) are attached directly to the sides of the rectangular device, which allows greater ZnS(Ag) mass fractions and better overall light collection. The second design is based on alternating layers of ZnS(Ag) and PMMA arranged orthogonal to the incident neutron beam. This design also employs SiPMs attached to the sides parallel to the beam.

By using SiPMs, the overall detector mass and volume is reduced, and the amount of Cherenkov radiation produced and collected is minimized. The results to follow indicate the devices proposed can discriminate against gamma-ray background with use of pulse-height discrimination alone, so that the complicated, pulse-shaping techniques previously used are no longer needed. In addition to their improved gamma-ray and Cherenkov rejection, the new detectors offer substantially improved fast-neutron detection efficiencies relative to the Hornyak button. The location of the SiPMs shortens the distance the light travels and leads to better collection of the isotropic scintillation light. As a consequence, a higher concentration of ZnS(Ag) and larger overall scintillator volumes can be used in both detectors (relative to the Hornyak button), thereby maximizing fast-neutron interactions and subsequent light production.

Ultimately, the goal of the study reported here was to provide a preliminary, numerical demonstration of these alternative detector designs. In what follows, the computational methodology and physics models used are detailed first. Then, application of these tools to the original Hornyak button and a comparison to experimental data for validation purposes are described. The development, modeling, and optimization of the two alternative detector designs are then reported, followed by concluding remarks.

2. Evaluation methods

2.1. Source terms

In the TREAT hodoscope, the detectors were in an environment comprised of neutrons and gamma rays. A review of past work suggested that gamma rays originated from multiple sources [3]. Prompt fission gamma rays were present with an intensity of approximately 5 per fission neutron. These gamma rays may contribute to the prompt signal used to identify fuel motion, but for the work described here, rejection of gamma rays was maximized. In addition to the prompt, fission gamma rays, neutron-activation gamma rays were generated by the capture of neutrons in the steel collimator with an intensity of about 9 additional

gamma rays per fission neutron. These neutron-activation gamma rays were modeled as the background radiation in the calculations.

Because it would be nearly impossible to simulate the original TREAT hodoscope environment, it was decided to define a representative neutron and gamma-ray radiation field that is believed to be conservative. Specifically, neutrons were assumed to be monodirectional and perpendicular to a detector's front face (i.e., the face adjacent to a collimator channel). Neutron energies were assumed to follow a ^{235}U thermal fission spectrum. For each source neutron incident on the detector, it was assumed that 10 gamma rays were *simultaneously incident* on the detector. These gamma rays were assumed to be isotropically distributed in angle and to follow a fission gamma-ray spectrum in energy [7]. Finally, the neutron and gamma-ray sources were assumed to be distributed uniformly in space over the detector's entire front face.

The responses of the three ZnS(Ag)-based detectors were represented by the detected optical photons (OPs). An optical photon that travels to the light-collection device was recognized as detected because of the high PMT and SiPM photon-detection efficiency [8] for optical photons following the ZnS(Ag) emission spectrum [9]. The self-absorption in ZnS(Ag) and other aspects of optical photon transport were taken into account as well.

2.2. Detector response and efficiency

A detector's responses to the incident neutrons and gamma rays were computed using separate simulations. Based on the number of detected optical photons in each pulse event, the signal and the background pulse-height spectra were formed. Indeed, the neutron-detection efficiency depended on the lower level discriminator (LLD) setting, which was represented by the number of detected optical photons in this study. However, based on the tallied gamma-ray spectrum, an appropriate LLD can be set to reject a majority of the background. The neutron-detection efficiency at this LLD setting was used as the criteria to evaluate each detector's performance.

Specifically, the detection efficiency ε at an LLD setting was computed based on the tallied pulse-height spectra as

$$\varepsilon = \frac{\text{Number of pulses with height larger than LLD}}{\text{Total number of pulses}}. \tag{1}$$

Corresponding to different LLD settings, the coupled neutron-detection efficiency and gamma-detection efficiency can be computed, with an associated signal-to-noise (S/N) ratio defined as

$$\text{S/N ratio} = \frac{\text{Neutron detection efficiency}}{\text{Gamma-ray detection efficiency}}. \tag{2}$$

In this paper, if not specified explicitly, the neutron-detection efficiency was defined using an LLD setting consistent with an S/N ratio of 100. It is understood an S/N ratio of 100 with respect to the background gamma rays is a desirable functional capability of advanced fast-neutron detectors for the hodoscope [10], and, hence, it is believed that the neutron-detection efficiency defined in this way is a practical value.

2.3. Physical models and approximations

All simulations were performed using Geant4 version 10.2 with patch 02. Neutron interactions were based on the neutron cross-section file G4NDL4.5. Nuclear processes were simulated using the recommended QGSP BERT HP physics list [11], and all necessary optical processes, e.g., optical absorption, scintillation, Cherenkov, and boundary interactions (using the UNIFIED model), were taken into account. For gamma-ray calculations, scintillation and Cherenkov processes were enabled independently so that scintillation noise, Cherenkov noise, and their combination were analyzed separately. The refractive index of PMMA is a known function of wavelength [12], with an average value of approximately 1.49. For ZnS(Ag), the refractive index was set to 2.36, while the mean free path of the optical photons in ZnS(Ag) was set to 13 μm [13]. The light yield of ZnS(Ag) was set to 37 optical photons per keV [14] with an emission spectrum maximized at a 450-nm wavelength [9]. For all cases, millions of source-particle events were simulated to obtain good statistics. A signal event contained one source neutron, while a noise event consisted of 10 incident gamma rays if not specified.

3. Hornyak button model

3.1. Model details

A model of the Hornyak Button was developed in Geant4, as shown in Fig. 2. The light guides were modeled as two sectors, each with a central angle of 160° [3]. To model the homogeneous mixture of ZnS(Ag) and PMMA in the scintillation volume, ZnS(Ag) grains were modeled as spheres with a radius of 20 μm [15]. Only the reported average radius was used because information for particle size distribution is not known from the literature. Based on a 5% mass fraction of ZnS(Ag) [3], the number of ZnS(Ag) grains N_g was computed. To randomly distribute the N_g grains into the scintillation volume, a pseudo-randomization method was used. The scintillation volume was divided into N_x, N_y, and N_z layers along the x, y, and z axes, respectively. The alignment of the scintillation volume with respect to the axes is shown in Fig. 1. The number of layers along an axis was proportional to the corresponding dimension of the scintillation volume, i.e.,

$$\frac{N_x}{L_x} = \frac{N_y}{L_y} = \frac{N_z}{L_z}, \tag{3}$$

where $L_x = 5/8$, $L_y = 7/64$, and $L_z = 1$ in. (see Fig. 1). These layers formed $N_x \times N_y \times N_z = N_g$ cells, and a cell contained one ZnS(Ag) grain. As computed, the numbers of layers are not integers, while the number of grains along an axis must be an integer. Hence, the scintillation volume was first divided into $\widetilde{N}_z$ layers along the z axis, where $\widetilde{N}_z$ was the integer part of N_z. Then, each z layer contained $\widetilde{N}_{xy} = N_g/\widetilde{N}_z$ grains. The values of N_x and N_y were recomputed by

$$\begin{aligned} \widetilde{N}_{xy} &= N_x \times N_y \\ N_x/L_x &= N_y/L_y. \end{aligned} \tag{4}$$

Then, the number of y layers in a z layer was sampled to be $\widetilde{N}_y + 1$ with probability $N_y - \widetilde{N}_y$ or $\widetilde{N}_y$ otherwise, where $\widetilde{N}_y$ is the integer part of N_y. The number of x layers was sampled in the same way. A ZnS(Ag) grain was randomly embedded in each cell if it did not overlap with the neighbor placed grains. If placement of a grain in a cell failed 100 times, i.e., all the sampled positions of the grain overlapped with the neighbor grains, that cell was left as void, and the number of placed grains was counted. The volume of the scintillation volume not occupied by the ZnS(Ag) grains (including the void cells) was filled with PMMA. This pseudo-randomization method avoided issues with overlapping ZnS(Ag) grains and ensured that desired mass fractions were preserved to within approximately 0.2% of the desired value for the cases studied. Fig. 2b shows the random distribution of the ZnS(Ag) grains of the model. In addition, a dummy, finite-volume PMT was connected to the end window of the Hornyak button (not shown in Fig. 2a). If an optical photon left the Hornyak button and entered the PMT region, the particle was killed, and the tally, i.e., number of detected optical photons in an event, was increased by one.

The outer surface of a ZnS(Ag) grain was modeled as ground, and the polished-front-painted surface finish in Geant4 [16] was used to model the optical reflective property of the outer surfaces of the light guides [3]. All other surfaces, e.g., the surfaces between the scintillation volume and the light guides and the surface between the Hornyak button and the PMT, were modeled as polished [3,17]. Because all the surfaces except the coupling ones in the Hornyak button were coated with white reflective paint [3], no surface absorption of optical photons was considered. All surfaces were assumed to be of the dielectric–dielectric type.

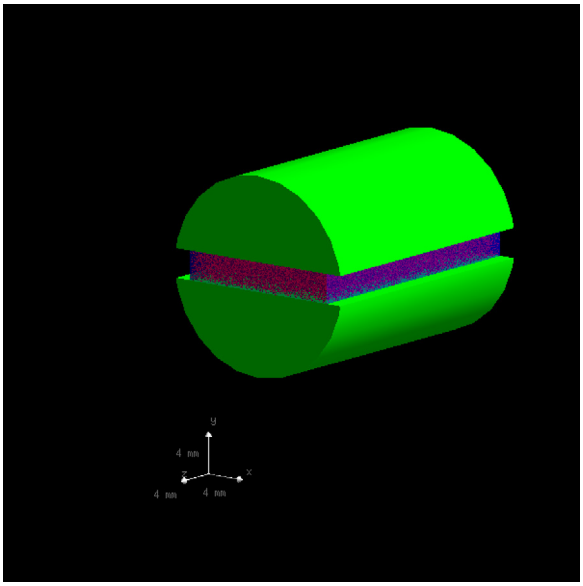

(a) Overall geometry.

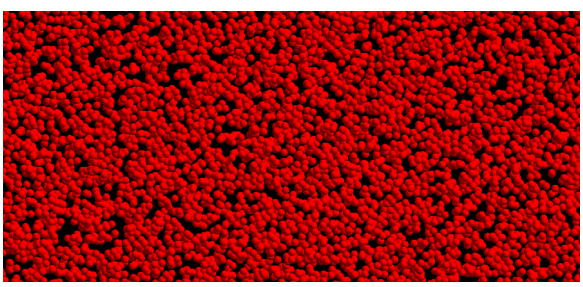

(b) Randomization of the ZnS(Ag) grains in the scintillation volume.

Fig. 2. The developed Hornyak button model in Geant4.

To simulate neutron responses, prompt neutrons were born uniformly in the cross-sectional plane of the scintillation volume (Fig. 3a). For gamma-induced scintillation, 10 gamma rays per source neutrons were also sampled uniformly across the cross-sectional plane of the scintillation volume. However, because Cherenkov radiation is generated in both the scintillation region and the light guides, incident gamma rays were sampled across the entire cross-sectional area of the Hornyak button (Fig. 3b) in order to simulate the response due to Cherenkov radiation. To maintain a consistent gamma-ray intensity between the two cases, the number of gamma rays per event for the Cherenkov study was

$$N = \frac{\text{Cross-sectional area of the detector}}{\text{Cross-sectional area of the scintillation volume}} \times 10 \approx 69. \quad (5)$$

3.2. Results

Fig. 4 shows the predicted pulse-height spectra and neutron-detection efficiencies for the Hornyak button. As indicated by Fig. 4a, the neutron pulse-height distribution is flatter than that of the scintillation noise, which makes pulse-height discrimination of the scintillation noise possible at reasonably low LLD settings. Contrarily, the intense Cherenkov noise is readily apparent and dominates the gamma-ray background. Fig. 4b shows that for a wide range of LLD settings, the neutron-detection efficiency is on the order of 0.1%. One factor causing the relatively low neutron-detection efficiency is the small amount of energy deposited in the scintillator. According to the calculation, on average, each neutron resulted in approximately 5-keV energy

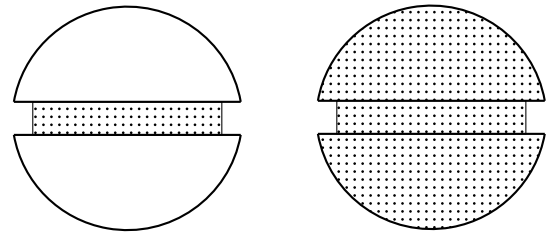

(a) Source plane 1. (b) Source plane 2.

Fig. 3. One neutron per event was generated uniformly in source plane 1. To evaluate the gamma-induced scintillation noise, 10 gamma rays per event were generated uniformly in source plane 1. To evaluate the gamma-induced Cherenkov noise and the combined Cherenkov-scintillation noise, 69 gamma rays per event were born uniformly in source plane 2.

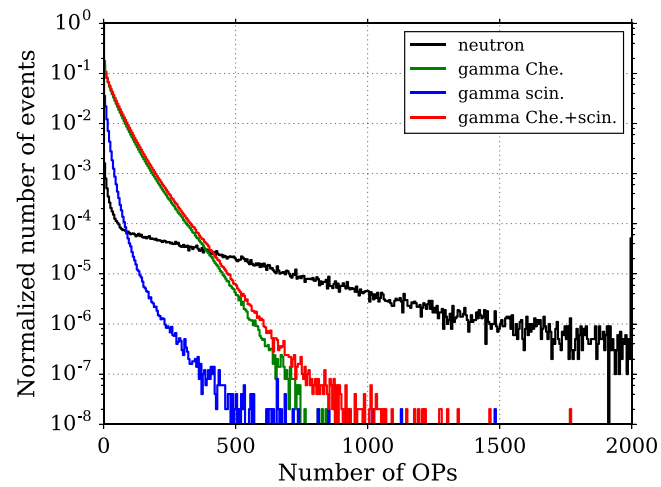

(a) Pulse-height spectra in different cases.

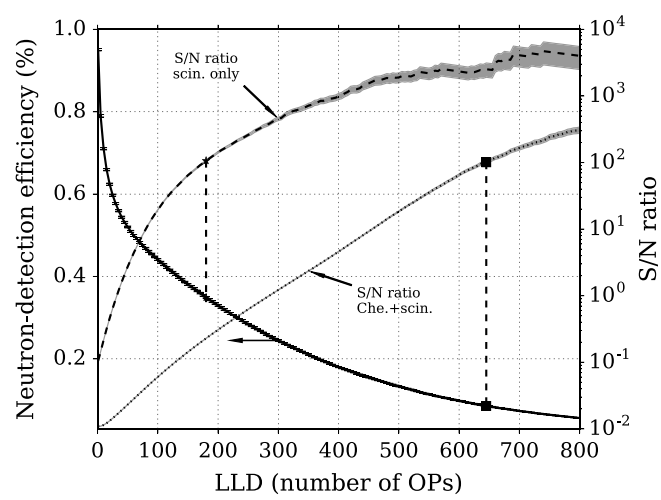

(b) Neutron-detection efficiency and corresponding S/N ratio as a function of LLD settings, included are the uncertainty bands with one standard deviation.

Fig. 4. Results of the original Hornyak button model.

deposited in the ZnS(Ag). This limited energy deposition may be due to the relative low concentration of the ZnS(Ag) in the scintillation volume, which results from the compromise between light generation and light absorption. Furthermore, if it is assumed the Cherenkov noise is rejected by the pulse-shaping technique, an LLD setting of 180 optical photons can achieve an S/N ratio of 100 with respect to gamma-induced

scintillation noise, and the corresponding neutron-detection efficiency is about 0.35%, as shown in Fig. 4b. It was reported that the neutron-detection efficiency of Hornyak button was approximately 0.1%, or, for neutrons above 0.1 MeV, the value is approximately 0.4% [3]. Hence, the simulated results are in relatively good agreement with the reported values, an agreement that provides some validation of the methodology used.

If both gamma-induced scintillation and Cherenkov contributions are included, to achieve an S/N ratio of 100, an LLD setting of 645 optical photons is necessary, and the corresponding neutron-detection efficiency is about 0.086%, as shown in Fig. 4b. In realistic application, the Cherenkov noise may even be stronger because it can also be generated in the glass envelope of the PMT [3] but was not considered in the calculation. Hence, the results verify the necessity of the pulse-shaping technique to reject the Cherenkov noise, which may contribute to the non-linear detector response with increased reactor power during transient experiments [3].

4. Design and optimization of Hornyak variants

Two variants of the Hornyak button were designed and optimized via numerical simulation; one, like the Hornyak button, is based on a homogeneous mixture of ZnS(Ag) and PMMA, while the other is based on alternating layers of ZnS(Ag) and PMMA. These detectors use SiPMs adjacent to the scintillation volumes to collect light, as shown in Fig. 5. The use of SiPMs is more efficient than the combination of light guides and the PMT used in the original Hornyak button. In the Hornyak button, the majority of the scintillation light needs to be reflected at the cylindrical surfaces of the light guides and may re-enter the scintillation volume several times to reach the PMT placed at the far end of the device (see Fig. 1). Each time the light passes through the scintillation volume, it may be absorbed by the relatively opaque ZnS(Ag). Thus, the useful concentration of the ZnS(Ag) in the scintillation volume is limited. In addition, although the PMMA light guide provides a relatively good light-collection efficiency [3], it also introduces significant mass and corresponding Cherenkov noise. A substantial amount of the Cherenkov light generated in the light guide can reach the PMT and cause overwhelming background noise without proper pulse-shape discrimination.

The two, proposed detectors differ in how their scintillation volumes are configured. For the layered detector, the scintillation volume consists of repeated layers of ZnS(Ag) and PMMA. The layered configuration is more efficient for the forward-directional, recoil protons to deposit energy in the ZnS(Ag) layers compared to the scintillation volume of the Hornyak button, where a proton may not encounter a randomly-distributed ZnS(Ag) grain along its path and, therefore, cannot generate a signal pulse.

The homogenized detector builds more directly on the original Hornyak button design, where the scintillation volume is a Hornyak button-like mixture of PMMA and ZnS(Ag). Because of the improved, SiPM-based light collection method, use of a higher concentration of ZnS(Ag) in the scintillation volume is possible, which increases overall light production and leads to better maximum performance. Due to the random distribution of the ZnS(Ag) grains, the scintillation volume of the homogenized detector is less efficient for the forward-directed protons to deposit energy in the scintillator than the layered detector. However, this inefficiency may contribute to improved gamma-ray rejection. As the ratio of background gamma rays to incident neutrons increases, the corresponding S/N ratio decreases faster for the layered detector than for the homogenized detector. Hence, the homogenized detector will exhibit better performance in a highly intense gamma-ray background environment (beyond what is actually expected in the hodoscope environment).

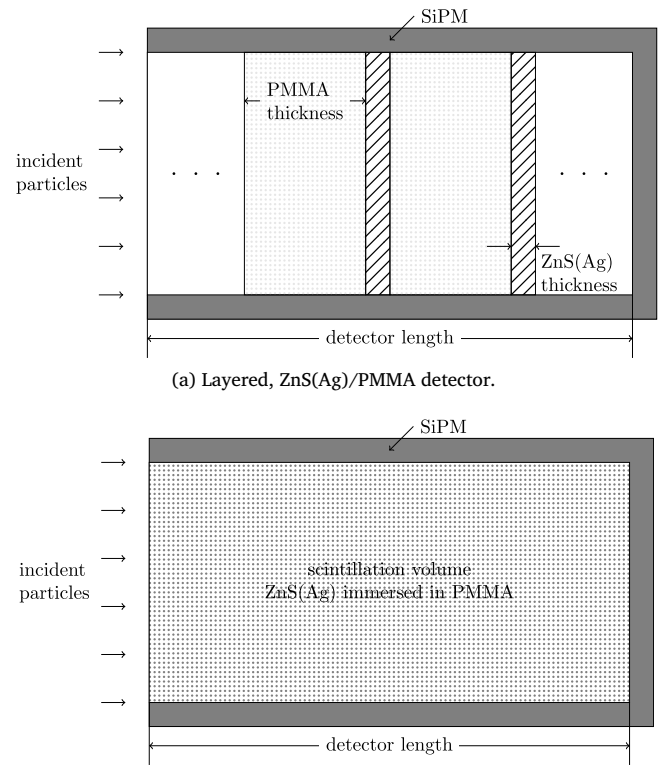

(a) Layered, ZnS(Ag)/PMMA detector.

(b) Homogenized, ZnS(Ag)/PMMA detector.

Fig. 5. Geometric illustrations of the two new detectors. The cross-sectional area of both scintillation volumes is a rectangle with size 2.51 × 8.89 mm, which is consistent with the designed channel slit in the TREAT hodoscope.

4.1. Layered, ZnS(Ag)/PMMA detector

The primary variables affecting the layered detector performance are the thicknesses of the PMMA and the ZnS(Ag) layers. While a thick PMMA layer enhances the proton generation and light collection, a large percentage of the recoil protons cannot escape the layer and are wasted. According to SRIM [18], the projected range of a 2-MeV proton in PMMA is about 65 μm. Additionally, a thick ZnS(Ag) layer is beneficial for maximizing the energy deposited by entering protons but leads to increased self-absorption of light. Hence, a parametric study was performed to find the optimal thicknesses of the PMMA and ZnS(Ag) layers for a representative 5-cm long layered device. The source particles were born uniformly in the detector's cross-sectional plane (a 2.52 × 8.89 mm rectangle). The ZnS(Ag) layers were modeled with ground optical surfaces, while the surfaces of the PMMA layers were modeled as polished.

Table 1 summarizes the PMMA and ZnS(Ag) layer thicknesses considered that can yield a neutron-detection efficiency above 2%. The gamma-induced noises by the scintillation and Cherenkov processes were used to set the LLD. The best case, where the thicknesses of the PMMA layer and the ZnS(Ag) layer are 0.18 mm and 12 μm, respectively, can yield an efficiency of about 3.31%.

Fig. 6 shows the pulse-height distribution and the neutron-detection efficiencies for a 5-cm long device with the optimum layer thicknesses. The gamma-induced noise is primarily introduced through scintillation, whereas the Cherenkov noise is minimal and easily rejected (Fig. 6a). In other words, a pulse-shaping technique as used for the Hornyak button is not necessary. Moreover, over a wide range of LLD settings, the neutron-detection efficiencies are larger than 1% (Fig. 6b). At an LLD setting of 180 optical photons, the S/N is predicted to be 100, including both

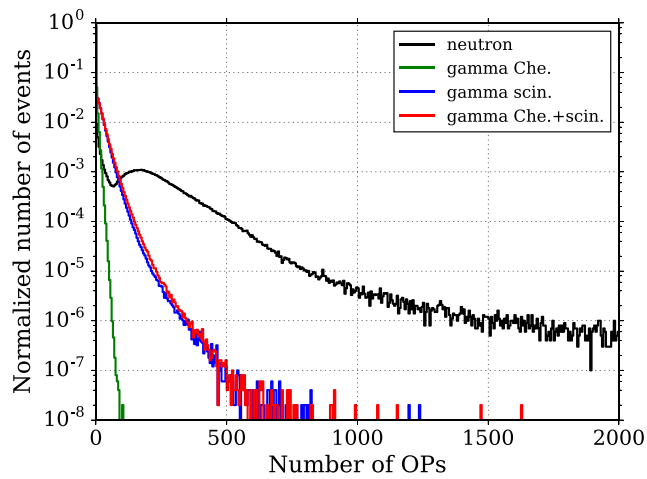

(a) Pulse-height distribution.

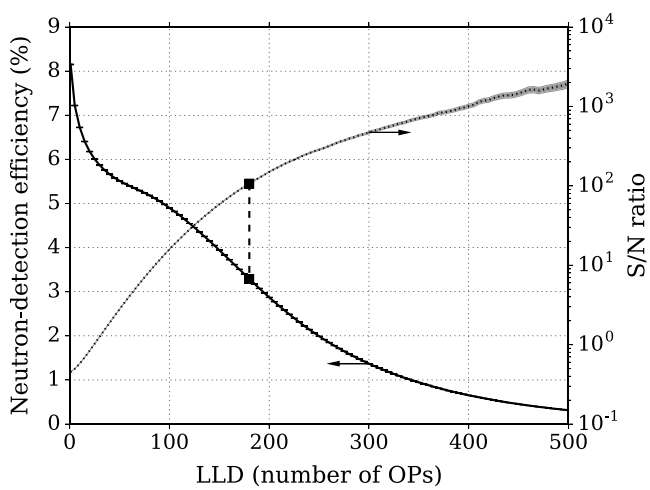

(b) Neutron-detection efficiency as a function of LLD settings. The corresponding S/N ratio (with uncertainty band) is also included.

Fig. 6. Performance of the 5-cm long, optimized layered detector.

Table 1
The neutron-detection efficiencies (%) of a 5-cm long, layered detector under different layer thicknesses.

PMMA (mm)	ZnS(Ag) (μm)						
	2	4	7	12	21	35	59
0.10	2.05	3.02	3.15	2.49	2.21		
0.18	2.44	3.03	3.26	3.31	2.71	2.06	
0.32		2.16	2.47	2.54	2.61	2.43	2.11

scintillation and Cherenkov, with a corresponding neutron-detection efficiency of approximately 3.31%.

Better efficiency is expected by increasing the length of the layered detector, and a study was performed to determine the neutron-detection efficiency as a function of the detector length with the PMMA and ZnS(Ag) layer thicknesses set to the best-case values; the results are shown in Fig. 7. At a length of one inch (the same length as the Hornyak buttons deployed at TREAT), the layered detector can yield a neutron-detection efficiency of approximately 1.8%. This improved performance (relative to the Hornyak button efficiency of 0.4%) may be explained by the increased energy deposition in the scintillator. At this length, the average energy deposited in ZnS(Ag) layers per source neutron was approximately 26 keV, which was larger than the energy deposited in the Hornyak button (approximately 5 keV). The results also indicate the

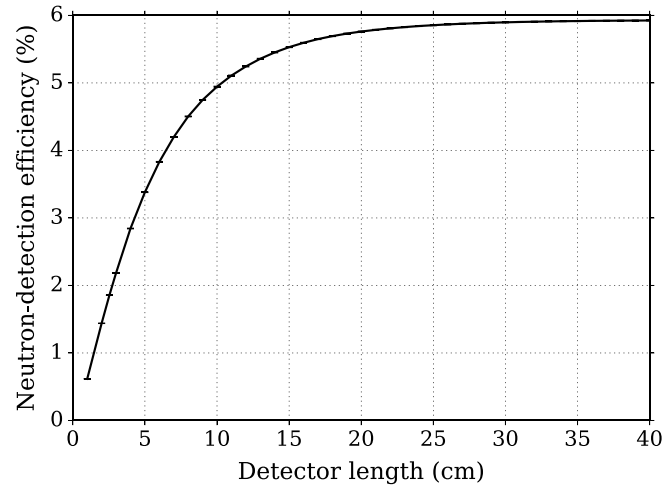

Fig. 7. Neutron-detection efficiency of the layered detector as a function of the detector length. The thicknesses of PMMA and ZnS(Ag) layers were set to 0.18 mm and 12 μm, respectively.

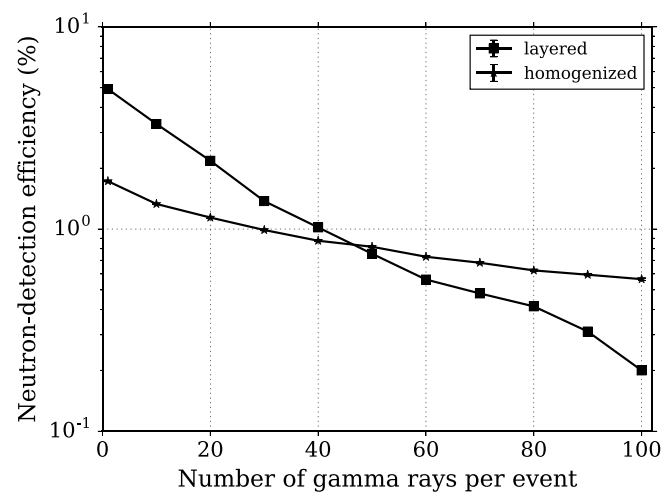

Fig. 8. A comparison of two new detectors' gamma-rejection capabilities.

neutron-detection efficiency saturates at just below 6.0% for a device with length larger than 20 cm. While better neutron-detection efficiency is expected from a longer detector, when selecting a length, one needs also to consider the size of SiPMs required, the overall space allocated for the detector and electronics, and the total cost of the resulting system.

The layered detector's gamma-rejection capability was evaluated by determining the neutron-detection efficiency as a function of the background gamma-ray intensity (whereas for all baseline work, a background intensity of 10 gammas per neutron was assumed). A 5-cm long device with optimal layer thicknesses was used. As the number of gamma rays per neutron was increased, a higher LLD setting was required to achieve an S/N ratio of 100. Hence, the neutron-detection efficiency decreases, as shown in Fig. 8. For up to 40 gamma photons per event, this detector can achieve a neutron-detection efficiency larger than 1%.

4.2. Homogenized, ZnS(Ag)/PMMA detector

The primary variable affecting the homogenized detector performance is the mass fraction of ZnS(Ag). Fig. 9 shows the impact of the ZnS(Ag) mass fraction for a 5-cm homogenized detector. At a mass fraction of 12%, a maximum neutron-detection efficiency of approximately 1.3% was achieved.

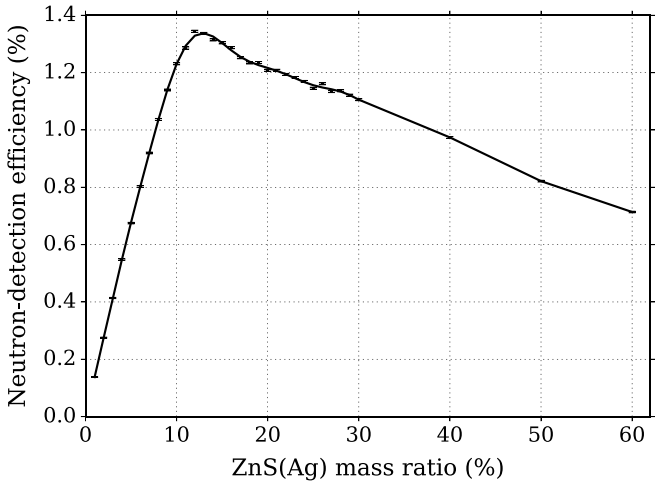

Fig. 9. Impacts of the ZnS(Ag) mass ratio in the scintillation volume on neutron-detection efficiency.

The pulse-height distribution and the associated neutron-detection efficiencies at different LLD settings of the best case are shown in Fig. 10. As also observed for the layered detector, Cherenkov noise can be readily rejected. At a LLD setting of 175 optical photons, the majority of the gamma-induced scintillation and Cherenkov noise can be discriminated to achieve an S/N ratio of 100, and the corresponding neutron-detection efficiency is about 1.3%.

The homogenized detector's efficiency as a function of detector length is shown in Fig. 11, for which the mass fraction of ZnS(Ag) was set to 12%. The results indicate the neutron-detection efficiency saturates at about 2.2%. To compare to the Hornyak button, at the length of one inch, the neutron-detection efficiency is about 0.8%. At this length, on average, one source neutron can result in approximately 12 keV deposited energy in the scintillator, which is larger than the 5 keV of the Hornyak button but less than the 26 keV of the layered detector.

The homogenized detector's gamma-rejection capability is illustrated in Fig. 8. Up to a gamma-to-neutron intensity ratio of about 20, this detector can achieve a neutron-detection efficiency above 1%. When the background exceeds 50 gamma rays per pulse event, the homogenized detector exhibits better performance than the layered detector. Hence, the homogenized detector is more resistant to gamma background, which may be explained by its overall lower efficiency.

5. Conclusion

Performance of three ZnS(Ag)-based scintillation detectors for the TREAT hodoscope – the Hornyak button and both layered and homogenized variants – was evaluated using Geant4. In the assumed, hodoscope-like neutron and gamma-ray environment, relatively good agreement was observed between the predicted Hornyak-button neutron-detection efficiency (approximately 0.35%) and previously reported values (between 0.1% and 0.4% depending on the neutron energy). The Hornyak-button model also confirmed that large levels of gamma-induced Cherenkov noise exist in the assumed radiation environment and, hence, that pulse-shape discrimination is, indeed, necessary. By collecting light at the transverse surfaces using SiPMs attached to the proposed devices, Cherenkov noise is reduced significantly, and gamma-induced scintillation and Cherenkov noise can be rejected by using simple pulse-height discrimination alone. For the same conditions, at the length of 5 cm, the optimized layered detector was predicted to have an improved neutron-detection efficiency of approximately 3.3%, while the optimized homogenized detector was predicted to have an efficiency of approximately 1.3%. By increasing the detector lengths, efficiencies were shown to saturate at about 5.9% and 2.2% for the layered and homogenized devices, respectively. For more intensive gamma-ray background (gamma-to-neutron ratios above 50), the homogenized detector exhibited better performance than the layered detector.

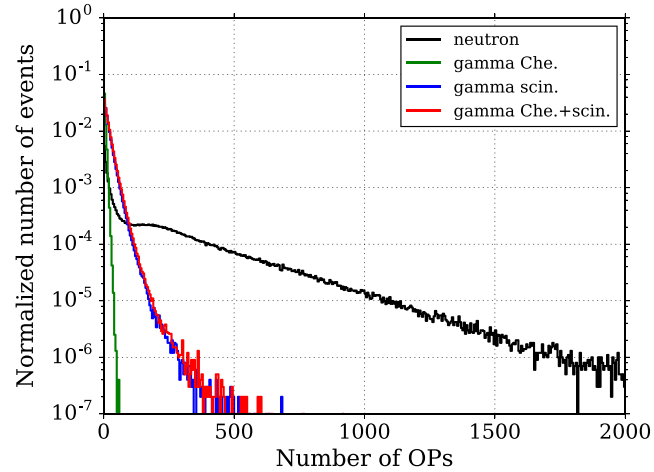

(a) Pulse-height distribution.

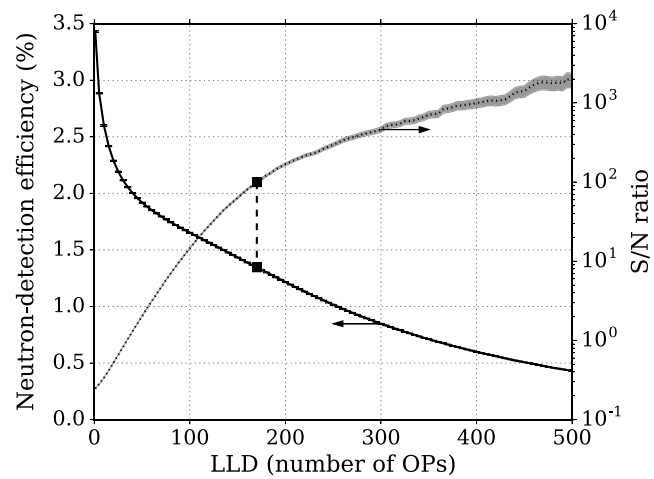

(b) Neutron-detection efficiency as a function of LLD settings. The corresponding S/N ratio (with uncertainty band) is also included.

Fig. 10. Performance of the 5-cm long, optimized homogenized detector.

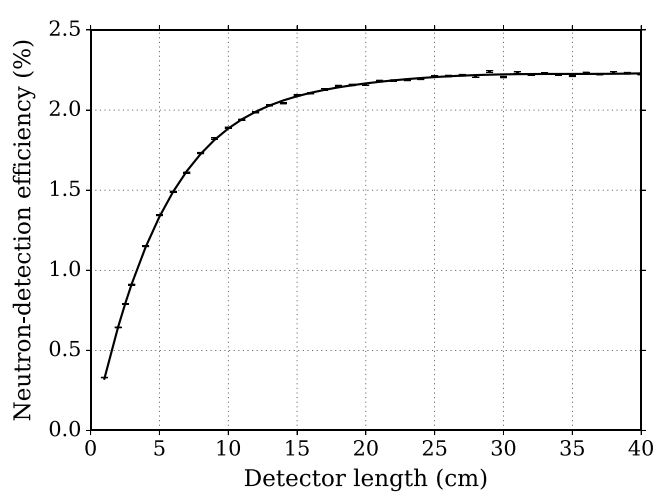

Fig. 11. Homogenized detector's performance as a function of detector length.

Ongoing efforts focus on the manufacturing of these detectors and testing them at the Kansas State University TRIGA Mark II research reactor.

Acknowledgments

The material presented is based upon work supported by the U.S. Department of Energy, Office of Nuclear Energy under Award Number DE-NE0008305. Some of the computing for this project was performed on the Beocat Research Cluster at Kansas State University, which is funded in part by NSF grants CNS-1006860, EPS-1006860, and EPS-0919443.

References

[1] J. Campell, Transient reactor test facility fact sheet, 2016. http://www4vip.inl.gov/research/transient-reactor-test-facility/d/transient-reactor-test-facility.pdf.

[2] V.K. Patel, M.A. Reichenberger, J.A. Roberts, T.C. Unruh, D.S. McGregor, MCNP6 simulated performance of Micro-Pocket Fission Detectors (MPFDs) in the Transient REActor Test (TREAT) facility, Ann. Nucl. Energy 104 (2017) 191–196.

[3] A. De Volpi, R. Pecina, R. Daly, D. Travis, R. Stewart, E. Rhodes, Fast-neutron hodoscope at TREAT: development and operation, Nucl. Technol. 27 (3) (1975) 449–487.

[4] W. Hornyak, A fast neutron detector, Rev. Sci. Instrum. 23 (6) (1952) 264–267.

[5] A. De Volpi, K. Porges, Rejection of gamma background radiation pulses in Hornyak Buttons, IRE Trans. Nucl. Sci. 9 (3) (1962) 320–326.

[6] P. Ghosh, W. Fu, R. Fronk, D.S. McGregor, J.A. Roberts, Evaluation of MSNDs for Fast-Neutron Detection and the TREAT Hodoscope, Trans. Amer. Nucl. Soc. 115 (2016) 1009–1012.

[7] J.M. Verbeke, C. Hagmann, D. Wright, Simulation of neutron and gamma ray emission from fission and photofission, Lawrence Livermore National Laboratory, Livermore CA, UCRL-AR-228518 3, 2010, pp. 25–35.

[8] B. Dolgoshein, V. Balagura, P. Buzhan, M. Danilov, L. Filatov, E. Garutti, M. Groll, A. Ilyin, V. Kantserov, V. Kaplin, et al., Status report on silicon photomultiplier development and its applications, Nucl. Instrum. Methods Phys. Res. A 563 (2) (2006) 368–376.

[9] BC702 data sheet. http://www.crystals.saint-gobain.com/sites/imdf.crystals.com/files/documents/sgc-bc702-data-sheet_70148.pdf.

[10] H.J.M. Chichester, Advanced fuels campaign in-reactor instrumentation overview, Oct. 28, 2015. https://www.energy.gov/sites/prod/files/2015/11/f27/7.

[11] Reference Physics Lists. http://geant4.cern.ch/support/proc_mod_catalog/physics_lists/referencePL.shtml.

[12] PMMA refractive index. http://refractiveindex.info/?shelf=organic&book=poly(methyl_methacrylate)&page=Szczurowski.

[13] ZnS(Ag) Scintillation Material, 2002. www.hep.ph.ic.ac.uk/fets/pepperpot/docs+papers/zns_602.pdf.

[14] Saint-Gobain Crystals scintillation products. http://www-eng.lbl.gov/~shuman/NEXT/MATERIALS&COMPONENTS/WLS_materials/Organics-Brochure.pdf.

[15] C. Fink, Optimization of a Hornyak-button detector for fast-neutron detection, IEEE Trans. Nucl. Sci. 29 (1) (1982) 718–721.

[16] Geant4 user's guide for application developers, December 4, 2015. http://geant4.web.cern.ch/geant4/UserDocumentation/UsersGuides/ForApplicationDeveloper/html.

[17] J. Nilsson, V. Cuplov, M. Isaksson, Identifying key surface parameters for optical photon transport in GEANT4/GATE simulations, Appl. Radiat. Isot. 103 (2015) 15–24.

[18] J.F. Ziegler, M.D. Ziegler, J.P. Biersack, SRIM–The stopping and range of ions in matter (2010), Nucl. Instrum. Methods Phys. Res. Sect. B 268 (11) (2010) 1818–1823.